Bioactive Materials 20 (2023) 561–573

Contents lists available at ScienceDirect

Bioactive Materials

journal homepage: www.keaipublishing.com/en/journals/bioactive-materials

Wound microenvironment self-adaptive hydrogel with efficient angiogenesis for promoting diabetic wound healing

Zijian Shao, Tianyu Yin, Jinbo Jiang, Yang He, Tao Xiang *, Shaobing Zhou **

Key Laboratory of Advanced Technologies of Materials, Ministry of Education, School of Materials Science and Engineering, Southwest Jiaotong University, Chengdu, 610031, PR China

ARTICLE INFO

Keywords:
Wound microenvironment
Self-adaptive hydrogel
MMP-9 responsive
Angiogenesis
Diabetic wound healing

ABSTRACT

Neovascularization is critical to improve the diabetic microenvironment, deliver abundant nutrients to the wound and promote wound closure. However, the excess of oxidative stress impedes the healing process. Herein, a self-adaptive multifunctional hydrogel with self-healing property and injectability is fabricated through a boronic ester-based reaction between the phenylboronic acid groups of the 3-carboxyl-4-fluorophenylboronic acid -grafted quaternized chitosan and the hydroxyl groups of the polyvinyl alcohol, in which pro-angiogenic drug of desferrioxamine (DFO) is loaded in the form of gelatin microspheres (DFO@G). The boronic ester bonds of the hydrogel can self-adaptively react with hyperglycemic and hydrogen peroxide to alleviate oxidative stress and release DFO@G in the early phase of wound healing. A sustained release of DFO is then realized by responding to overexpressed matrix metalloproteinases. In a full-thickness diabetic wound model, the DFO@G loaded hydrogel accelerates angiogenesis by upregulating expression of hypoxia-inducible factor-1 and angiogenic growth factors, resulting in collagen deposition and rapid wound closure. This multifunctional hydrogel can not only self-adaptively change the microenvironment to a pro-healing state by decreasing oxidative stress, but also respond to matrix metalloproteinases to release DFO. The self-adaptive multifunctional hydrogel has a potential for treating diabetic wounds.

1. Introduction

Diabetes mellitus shows a high prevalence around the world and about 19–34% of diabetic patients are predicted to develop complications such as diabetic wounds, which turn into a critical threat to the health and life of the patients [1]. Unlike four overlapping processes of hemostasis, inflammation, proliferation, and re-epithelialization for acute wound healing [2], diabetic wound reveals complicated characteristics that delay the healing process. Large amounts of reactive oxygen species (ROS) from oxidative stress, increased expression of pro-inflammatory cytokines, and bacterial infection impel the wound to become a continuous inflammatory microenvironment [3–6]. Overexpression of the matrix metalloproteinase-9 (MMP-9) in the diabetic wound microenvironment impairs wound healing by weakening the formation of granulation tissue and inactivating growth factors [7,8], which acts as the primary gelatinase after wounding and participates in extracellular matrix (ECM) degradation and tissue reorganization [8]. In addition, hyperglycemia-induced inadequate vascularization limits the input of nutrients and oxygen to the wound sites, thus delaying wound healing [9,10]. These features impair the growth factors needed for wound healing, forming a negative microenvironment of diabetic wound healing. Materials like hydrogels with microenvironment-responsive ability could achieve a stimuli-responsive drug release on demand and biodegradation affected by the microenvironment. Thus, they are applied in several biomedical applications such as tumor therapy [11], brain injury [12], and bone healing [13]. On the other hand, the wound microenvironment is dynamically changed with the repair process, in which pH value, biological cues such as growth factors and cytokines are included. The functions of hydrogel should change with the dynamical microenvironment. Therefore, it's urgent to develop a multifunctional hydrogel which cannot only accelerate wound healing by taking advantage of the microenvironment, but also possess self-adaption to dynamically regulate and respond to the wound microenvironment.

Peer review under responsibility of KeAi Communications Co., Ltd.
* Corresponding author.
** Corresponding author.
E-mail addresses: xita198906@swjtu.edu.cn (T. Xiang), shaobingzhou@swjtu.edu.cn (S. Zhou).

https://doi.org/10.1016/j.bioactmat.2022.06.018
Received 11 April 2022; Received in revised form 7 June 2022; Accepted 25 June 2022

One of the most efficient ways to directly deliver therapeutics for wound healing is wound dressing therapy. Wound dressings, such as electrospun nanofibers, polyurethane-based film, porous foams and functional hydrogels have been introduced to accelerate the healing process [14–18]. Hydrogels have drawn much attention since they can absorb wound exudate, maintain moisture at the wound sites and possess a suitable modulus that matches the soft tissues [19–21]. During the past years, hydrogels with multiple functions such as ROS-scavenging, antibacterial property, regulation of the immune cells, and promoting angiogenesis have been designed to modulate the microenvironment of the wound [18,22–25]. However, the integrity of the hydrogels is easy to be destroyed when exposed to normal movement and local pressure [26]. The self-healing capacity of the hydrogels has attracted much attention due to their many similarities to the ECM, which can self-heal after minor injuries [27,28]. Furthermore, the injectability can be realized through the self-healing capacity, allowing the hydrogel can smoothly fill the deep or irregular-shaped wound [29]. Consequently, endowing the hydrogel dressings with self-healing capability and injectability is crucial for designing functional wound dressings.

Self-healing capacity provides hydrogel with the guarantee of integrating its fragments and maintaining functional integrity. Reversible interactions are regarded as an efficient way to induce hydrogel with not only proper mechanical strength but also outstanding self-healing capability, which is coincident with the demand for wound dressings [30,31]. Serval types of covalent and non-covalent interactions including Schiff base, boronic ester bonds hydrogen bonds, ionic bonds, and coordinate bonds have been applied to design self-healing hydrogel dressings [32–36]. Among them, boronic ester bonds possess the characteristics that they can respond to high concentrations of glucose and hydrogen peroxide (H_2O_2), which matches consistently with the microenvironment of diabetic wounds. However, the formation of the diol-boronic acid complex relies on the pKa of the boronic acid, in which most of the boronic acids have pKa values > 8. In consequence, the utility in physiologic conditions of these materials is limited. The substituent of fluorine on benzene can decrease the pKa [37]. To meet the needs of wound dressings for diabetic wounds, 3-carboxyl-4-fluorophenylboronic acid (FPBA) with pKa of ~7.2 can be introduced, in which the phenylboronic acid groups of the FPBA-grafted quaternized chitosan (QCSF) and the hydroxyl groups of the polyvinyl alcohol (PVA) bonded to form hydrogel networks to maintain stability on diabetic wound sites. In addition, the pH of skin tissue is below 7.0 after the wound healing process. The hydrogel can be disassembled to avoid residue on account of the destruction of the diol-boronic acid complex under a lower pKa value.

In this work, we developed a wound microenvironment self-adaptive multifunctional hydrogel based on boronic ester bonds between the QCSF and PVA, which was named as QCSFP (Fig. 1a). The boronic ester bonds in the hydrogel which contains desferrioxamine loaded gelatin microspheres (DFO@G) could react with the hyperglycemia and over-expressed ROS to regulate the microenvironment and release DFO@G microspheres. The microspheres could respond to the highly expressed MMP-9 to achieve a controlled release of desferrioxamine (DFO). Additionally, released DFO acted as a Fe^{2+} chelator to interfere with the required prolyl-hydroxylases cofactor, which was the critical factor in the process of hypoxia inducible factor-1 (HIF-1α) degradation [38]. Simultaneously, the ROS was further suppressed owing to the chelation. Thus, the modification of p300 by methylglyoxal was reduced, and p300 could up-regulate the expression of HIF-1α and its downstream vascular endothelial growth factor (VEGF), thereby facilitating angiogenesis [39]. Through dynamically responding and decreasing oxidative stress of the diabetic wound by self-adaption of DFO@G-QCSFP hydrogel, DFO@G and subsequent DFO were released on demand to promote angiogenesis to accelerate the diabetic wound healing (Fig. 1b).

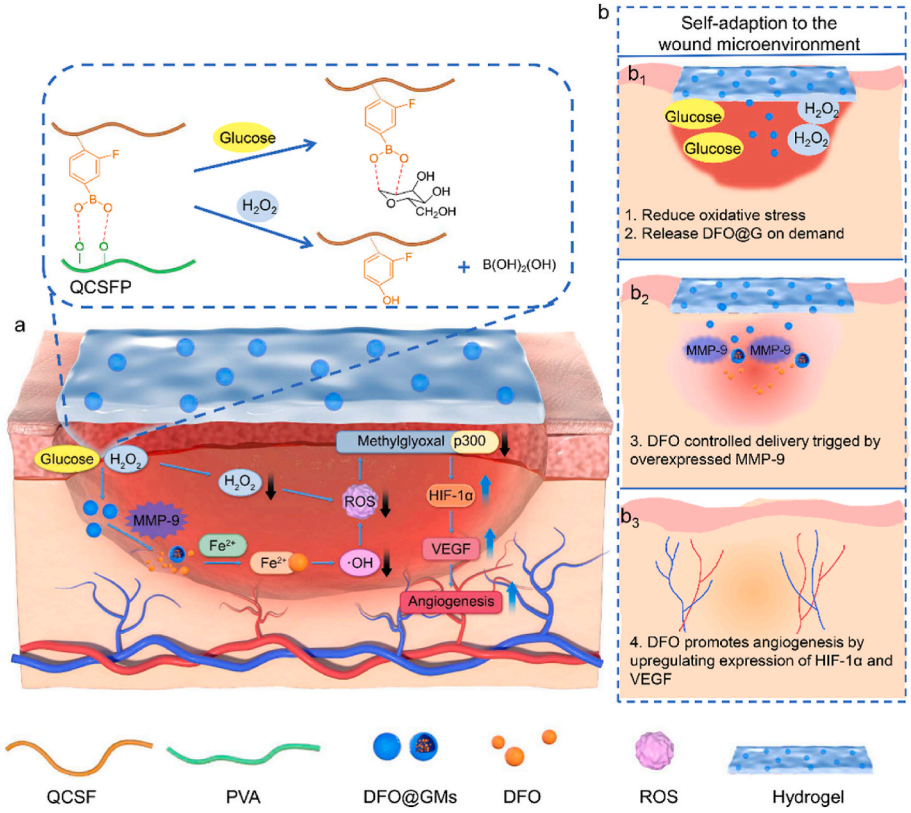

Fig. 1. The fabrication and application of self-adaptive DFO@G-QCSFP for accelerating diabetic wound healing on the full-thickness diabetic wound of a diabetic SD rat. a) The chemical structure of the hydrogel and the mechanism of the hydrogel for accelerating diabetic wound healing. b) The self-adaption of the hydrogel to wound microenvironment. The hydrogel reduced oxidative stress and released DFO@G on demand. Then DFO was released and promoted angiogenesis.

2. Experimental

2.1. Materials

Chitosan (CS, 100–200 mPa s, Mw: 2000 kDa, Macklin), 2,3-epoxypropyltrimethylammonium chloride (GTMAC, 80 wt% in water, Huaxia Reagent), FPBA (98%, Aladdin), PVA1788 (98%, Mw:56000, Adamas), gelatin (98%, Adamas), DFO (Sigma-Aldrich), genipin (Aladdin), streptozotocin (STZ, Sigma-Aldrich), sorbitan monooleate, (Span-80, Aladdin), acetone (AR, Kelong), ethanol (AR, Kelong), H_2O_2 solution (30 wt%, Kelong), sodium chloride (NaCl, 98%, Kelong), titanyl sulfate (96%, Aladdin) and methylene blue (MB, 98%, Kelong), sodium hydroxide solution (NaOH, 98%, Kelong), hydrogen chloride solution (HCl, 37%, Kelong), glycine (99%, Kelong), acetic acid (99%, Kelong), ethanol (96%, Kelong), ninhydrin (AR, Kelong), N-hydroxysuccinimide (NHS, 98%, Aladdin), N-(3-dimethylaminopropyl)-N′-ethylcarbodiimide hydrochloride (EDC·HCl, 98%, Aladdin), dimethyl sulfoxide (DMSO, AR, Kelong), citric acid monohydrate (AR, 99.5%, Aladdin), tin chloride dihydrate ($SnCl{\cdot}2H_2O$, 99%, Aladdin) and ethylene glycol monomethyl ether (ACS, 99.5%, Sigma-Aldrich) were received. 2,7-dichlorofuor-escin diacetate (DCFH-DA, Beyotime), Hoechest 33342 (97%, Sigma-Aldrich), dihydroethidium (DHE, Sigma-Aldrich) were obtained and used for experiments. All other chemicals were analytical reagents. Deionized (DI) water was used throughout the study.

2.2. Synthesis of QCSF

Quaternized chitosan (QCS) was synthesized according to a previous literature [40]. Briefly, 5.00 g CS powders were suspended in 180 mL deionized water, then 0.94 g glacial acetic acid was added. Subsequently, 6.40 g GTMAC was dropped slowly into the solution, then the reaction was stirred for 21 h at 55 °C. After that, the solution was centrifuged (6500 rpm, 8 min). The supernatant was precipitated with pre-cold acetone. The whole purification process was repeated 3 times, and the collected product was dried in a vacuum oven. The chemical structure was characterized by ^{1}H nuclear magnetic resonance (^{1}H NMR) and Fourier transform infrared spectroscopy (FTIR).

QCSF was synthesized by an amide reaction between the QCS and FPBA. Briefly, the QCS powders were dissolved in 300 mL phosphate buffered saline (PBS) and the pH was adjusted to 5.5. Meanwhile, 1.27 g FPBA, 2.39 g NHS and 3.98 g EDC were dissolved in 180 mL DMSO and the solution was stirred at room temperature for 4 h. Then two solutions were mixed and the reaction was carried out at room temperature for 36 h. The solution was lyophilized after dialysis and the FPBA-grafted quaternized chitosan (QCSF) was obtained. The ^{1}H NMR and FTIR of QCSF were performed as well. The grafting ratios of QCS and QCSF were calculated by the peak integral area ratio using equation (1) and equation (2) following:

$$QCS\ Grafting\ ratio\ (\%) = \frac{AH_b}{AH_1} \times 100\% \quad (1)$$

$$QCSF\ Grafting\ ratio\ (\%) = \frac{AH_{e1\sim e3}}{AH_1} \times 100\% \quad (2)$$

2.3. Evaluation of pKa of the QCSF

The pKa value of the QCSF polymer was measured by titration [41]. In each case, 50 mg of QCSF was dispersed in 50 mL of deionized water, and the pH was adjusted to 3 by 0.1 M HCl solution. Then 0.01 M NaOH was added to the solution to adjust the pH. The value of pKa was determined as the inflection point of the titration curve.

2.4. Preparation and characterization of DFO@G

DFO@G were prepared through a post-crosslinking strategy by genipin after an emulsification-solvent extraction [42]. Briefly, 0.001 g DFO and 1.50 g gelatin powders were dissolved in 10 mL DI water at 60 °C. Then the aqueous phase was dropped into 100 mL corn oil containing 1 wt% Span-80 and emulsified for 20 min. The whole mixture was cooled at 7 °C and stirred for 30 min. Subsequently, 150 mL acetone was added to dehydrate for 30 min. Then, the organic solvent was removed by suction filtration and the gelatin microspheres (GMs) were dried in a vacuum oven at room temperature. To prepare DFO@G, 50 mg dried GMs were suspended in 4 mL PBS, in which 1% w/v genipin solution was added and the crosslinking process was carried out for 12 h. After being washed by ethanol, the DFO@G were obtained. The particle sizes of GMs and DFO@G were recorded by optical microscope (Carl Zeiss Observer 7, Germany) and manually analyzed by Nano Measurer 1.2 software.

2.5. Fabrication and characterization of the injectable hydrogels

The injectable hydrogel was fabricated by mixing 5% w/v QCSF solution, 10% w/v PVA solution and 1 mg DFO@G. The obtained hydrogel was defined as DFO@G-QCSFP. For the control experiments, DFO directly loaded hydrogel and drug-free hydrogel were prepared using the same method, which were defined as DFO-QCSFP and QCSFP, respectively. The FTIR spectra were characterized on a Nicolet 5700 spectrophotometer to determine the chemical structure of the hydrogel. The distinct 3D porous structures of the hydrogels were observed by a Phenom Pro scanning electron microscope (SEM).

2.6. Rheological properties of the hydrogels

Rheometer (HAAKE RheoStress 5000, Germany) was applied to evaluate the rheological properties of the hydrogels. The experiment temperature was set to 37 °C and the storage modulus (G′) and loss modulus (G″) were investigated by putting the hydrogel on a parallel plate with a 20 mm diameter and a 1 mm gap. Strain amplitude sweep tests were applied to detect the critical strain point of QCSFP and DFO@G-QCSFP hydrogel with a frequency of 1 rad s^{-1}. Frequency sweep tests were conducted at a 1% strain amplitude.

2.7. Self-healing and injectable properties of the hydrogels

The self-healing ability of the hydrogel was evaluated by both macroscopic and quantitative experiments. For macroscopic tests, the hydrogel block was cut into two pieces, which were then put together and placed in a humidor at 25 °C for 2 h to observe. In addition, two-colored hydrogel blocks were blended for 2 h and stretched by tweezers. All the situations of the hydrogels were photographed. Furthermore, quantitative tests of QCSFP and DFO@G-QCSFP hydrogel were investigated by using the rheometer. The experiment was performed by using a time sweep test at 37 °C with a frequency of 1 rad s^{-1}. Strains were switched from small strain ($\gamma = 1\%$, 300 s for each interval) to large strain ($\gamma = 500\%$, 100 s for each interval), and 3 cycles were carried out. QCSFP hydrogel was prepared and loaded into a syringe then injected into a mold to recover their shapes. The injection processes were videotaped and photographed. To quantitatively analyze the shear-thinning properties of hydrogels, the rheometer was applied to detect the viscosity and shear-thinning behaviors of the hydrogel.

2.8. Responsive degradation behavior of the hydrogels

Since the boronic ester-based hydrogel was sensitive to stimuli of pH and glucose, the hydrogel was added to the PBS with different pH values (7.8 and 6.0, representing non-healing wound and healed wound, respectively [43]) and 16.6 mM glucose to simulate the responsive

degradation behavior under diabetic wound environment at 37 °C. The remaining samples were collected, dried and weighed at different intervals, and the remaining hydrogel was calculated by the following equation:

$$Remaning\ hydrogel\ (\%) = \frac{W_t}{W_0} \times 100\%$$

where W_t and W_0 are the dry weight of remaining hydrogels after degradation at different time points and the initial dry weight of the hydrogels, respectively.

2.9. MMP-9 responsive drug release analysis

In vitro drug release experiments were conducted to investigate the drug release property of the drug delivery system based on gelatin microspheres when responding to MMP-9. Briefly, 5 mg DFO@G was added to prepare hydrogel with drug-loaded microspheres. Then the prepared hydrogel was added to 4 mL of PBS solution containing 100 ng mL^{-1} MMP-9 to simulate the microenvironment of diabetic wounds [44,45]. At predetermined time intervals, 300 μL of the supernatant was collected, followed by addition of 7.5 μL $FeCl_3$ solution, then 300 μL of fresh PBS buffer with MMP-9 was added to maintain a constant volume. The concentrations of the DFO released from hydrogel were analyzed by UV–vis spectra using a Shimadzu UV-2550 spectrophotometer at 485 nm. Meanwhile, the drug release behavior of the direct drug-loaded hydrogel DFO-QCSFP and the DFO@G-QCSFP hydrogel without MMP-9 were investigated and analyzed.

2.10. ROS-scavenging ability evaluation

Titanyl sulfate (0.03 M) was used for evaluating the ROS-scavenging ability of the hydrogel [46]. The standard curve of different concentrations of H_2O_2 was established. Then the H_2O_2 solution (1 mM, 3 mL) was incubated with the 200 μL/500 μL hydrogel for different periods. At different time points, the supernatants (100 μL) were collected and 30 μL titanyl sulfate was added. Subsequently, the absorbance spectra of the above mixture solutions were measured to determine H_2O_2 concentrations. The ·OH scavenging capacity of the hydrogel was also investigated. Briefly, methylene blue (0.1 mg mL^{-1}) was added into a ·OH containing solution, which was produced by a Fenton reaction between H_2O_2 (1 mM) and Fe^{2+} (0.2 mg mL^{-1}). Subsequently, the ·OH solution was incubated with or without the hydrogel for different time intervals. The supernatant (100 μL) was collected and the absorption of the supernatant at 666 nm was recorded. The effect of concentration of DFO on ·OH scavenging was also evaluated.

2.11. Cytocompatibility of the hydrogel

Alamar Blue (AB) and Live/Dead assays were conducted to evaluate the effect of DFO@G and DFO@G-QCSFP hydrogels on cell viability and proliferation. Briefly, human umbilical vein endothelial cells (HUVECs) were seeded in a 48-well plate at a density of 1×10^4 cells per well. After the HUVECs adhered to the plate for 24 h, 500 μL of the sample was added into each well to incubate for different time intervals. Finally, cell viabilities were quantified using AB assay and normalized to the control group. Then, Live/Dead staining was performed by using a 12-well plate with a density of 2×10^4 cells per well. After cells adhered to the plate for 24 h, 500 μL hydrogel was added and incubated for different time intervals. After staining with 500 μL of calcein-AM/propidium iodide dye for 15 min, cells were observed under a fluorescent microscope (Carl Zeiss Observer 7, Germany) for the green and red fluorescence.

2.12. Effective DFO concentration determination

To determine the effect of DFO concentration on cytocompatibility, DFO with different concentrations was incubated with HUVECs and AB assay was performed to confirm the cell compatibility to HUVECs. The cells were seeded to a 48-well plate at a density of 2×10^4 cells per well, then the cells were cultured in DMEM supplemented with 10% FBS containing different concentrations of DFO (1, 3, 6 and 9 μM). On day 0, day 1, day 3, and day 5 of culture, 200 μL of 10% AB solution was added into each well and the cells were further cultured for 4 h, after the absorbance of each cell was measured at 570 and 600 nm with a UV spectrophotometer. A tube formation assay was conducted to investigate the effect of different concentrations of DFO on angiogenesis. In detail, 40 μL of Matrigel was added in a 96-well followed by gel under 37 °C for 30 min. Then 1×10^4 cells were added onto Matrigel and media containing different concentrations of DFO (0, 1, 3, 6 μM) were used. After 4 h incubation, optical microscopy (Leica DMR HCS, Germany) was employed to observe the tube formation. Nodes and tubes of each group were counted using Image J software. Combined with the results of cell proliferation and tube formation experiments, an effective concentration of DFO was determined.

2.13. Intracellular ROS-scavenging evaluation

The ROS-scavenging abilities of the hydrogels at cell levels were evaluated using the DCFH-DA probe. In short, HUVECs were seeded on 48-well plates for 24 h with followed by treatment with different hydrogels containing 100 μM H_2O_2 while the control group only treated with 100 μM H_2O_2. Cells treated with PBS served as negative group. Following treatment for 24 h, cells were rinsed with PBS and stained for 20 min with DCFH-DA and Hoechst. The ROS-scavenging ability of each group was imaged using fluorescence microscopy, and the mean fluorescence intensity was quantified by ImageJ.

2.14. In vivo diabetic wound healing assessment

Diabetic rats were induced by a method of intraperitoneal injection of STZ into healthy rats according to a previous literature [47]. After 16 h of fasting subjects, 25 male SD rats were induced by intraperitoneal injection of STZ (55 mg kg^{-1}) dissolved in pH 4.5 citrate buffer. Then blood glucose was measured every 3 d. The rats with blood glucose concentration greater than 16.6 mM after 4 weeks were determined as diabetic rats. The dorsal hairs of 20 diabetic rats were firstly shaved. Two full-thickness skin wounds with 10 mm diameter were made on the back of each rat. The diabetic rats were randomly divided into 4 groups and treated with: control, QCSFP, DFO-QCSFP, DFO@G-QCSP. The wound sites were treated and observed every three days and photographed on day 0, 3, 7, 10, 14, and 20 post-wounding. Wound areas in each group were measured and analyzed using the Image J software. The wound contraction rate was calculated by the following equation:

$$Wound\ contraction\ (\%) = \frac{(S_0 - S_n)}{S_0} \times 100\%$$

where S_0 and S_n represent the initial wound area and wound area at different time points, respectively. All animal experiments were carried out according to the guidelines approved by the Institutional Animal Care and Use Committee of Southwest Jiaotong University (No. SWJTU-2013-008).

2.15. In vivo ROS-scavenging ability evaluation

Rats were sacrificed and the regenerated skin samples were excised and collected on day 1 and day 3 to evaluate the in vivo ROS-scavenging ability. The in vivo ROS- scavenging was assessed by dihydroethidium (DHE) assay. In short, after washed in PBS, the frozen tissue sections were stained with DHE for 30 min. The in vivo ROS-scavenging ability was imaged using fluorescence microscopy, and analyzed by ImageJ.

2.16. Histology and immunohistochemistry

Rats were sacrificed and the regenerated skin samples were excised and collected on day 10 and day 20. The skin samples were fixed in 10% paraformaldehyde, dehydrated in gradient alcohol, and embedded in paraffin. Briefly, 5 μm sections were prepared for Hematoxylin-eosin (H&E) and Masson trichrome (MT) staining. Image J software was applied to determine the proportion of collagen deposition by measuring the intensity of the blue areas. For immunohistochemical (IHC) evaluation, the skin wound tissues were also excised on day 10 and day 20 post-surgery. To assess the effect of DFO on angiogenesis, the IHC method was used to detect CD31, α-smooth actin (α-SMA), VEGF and HIF-1α. In addition, the IHC staining of MMP-9 and Ki67 was also applied to detect the change of the wound microenvironment. The quantification of IHC was counted by Image-Pro Plus software.

2.17. Statistical analyses

All the experimental data were statistically analyzed and the results were expressed as a mean ± standard deviation. One-way ANOVA was used to measure differences for more than two groups with SPSS, version 24 (IBM). Data were considered as statistically significant difference when $*p < 0.05$, $**p < 0.01$, $***p < 0.001$ and $****p < 0.0001$ versus the indicated group.

3. Results and discussion

3.1. Fabrication of the wound microenvironment-responsive hydrogel

Wound dressings with multifunctional properties are highly desired owing to the complicated wound healing process [3,48]. To optimize the promotion of wound healing through wound dressing, a kind of wound environment self-adaptive multifunctional hydrogel dressing based on boronic ester was prepared (Fig. 2a). CS is known for its abundant biomedical advantages such as a variety of modifications, antimicrobial ability, and hemostatic activity. However, the limited solubility in water impedes its further applications. Compared to CS, QCS could efficiently improve the water solubility, which broadened the applications. PVA possesses a large number of hydroxyl groups, which favored the formation of boronic ester bonds compared to sodium alginate and dextran with a certain content of phenylboronic acid groups. Additionally, both quaternized chitosan and PVA have good biocompatibility [49,50]. As shown in Figure S1, GTMAC was firstly grafted on the side chain of the chitosan to prepare QCS. QCSF was synthesized by grafting FPBA on the QCS chain. The hydrogel was formed by the chemical crosslinking of boronic ester bonds between boric acid groups of QCSF and hydroxyl groups of PVA. The structures of QCS and QCSF were measured and confirmed by ^{1}H NMR (Figure S2 and S3), the grafting ratios of QCS and QCSF were 70% and 20%, respectively. The pKa of QCSF was measured and the value was 6.78 (Figure S4). DFO@G microspheres were then prepared through a post-crosslinking process. The optical microscope image in Fig. 2b confirmed that the DFO@G had a good dispersion. In

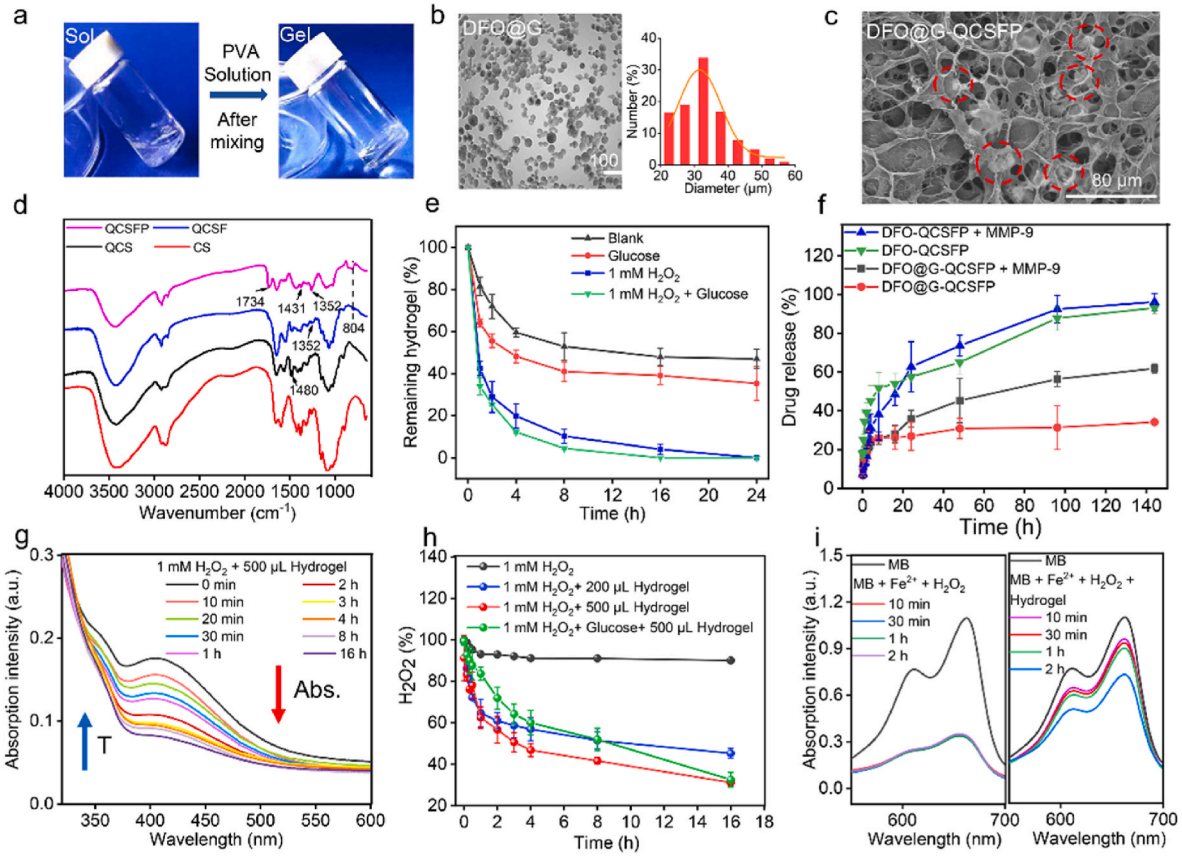

Fig. 2. Fabrication, responsibility, degradation and ROS scavenging of the multifunctional hydrogel. a) Optical images of the formation of QCSFP hydrogel based on boronic ester bonds. b) Optical microscope image and particle size statistics of the DFO@G. c) SEM images of the DFO@G-QCSFP hydrogel. d) FTIR spectra of the CS, QCS, QCSF, and QCSFP hydrogel. e) Degradation profile of the DFO@G-QCSFP hydrogel in simulated diabetic wound microenvironment (16.6 mM glucose and 1 mM H_2O_2) at 37 °C. f) DFO released from DFO@G-QCSFP with addition of MMP-9. g) UV–vis absorbance spectra of the H_2O_2 solution incubated with DFO@G-QCSSFP hydrogel within different time intervals. h) The H_2O_2 scavenging experiment in solutions incubated without or with the hydrogel. i) UV–vis absorbance spectra of MB degradation with or without the hydrogel triggered by Fenton reaction induced by Fe^{2+} and H_2O_2.

addition, the average size of microsphere was counted and the value was 32.56 ± 1.09 μm as shown. Compared to GMs in Figure S5a, the average size of DFO@G was reduced, which was attributed to the increase in the degree of crosslinking (Figure S6). The encapsulation efficiency and drug loading capacity of the DFO@G were evaluated as shown in Table S1. The SEM image in Fig. 2c shows that the DFO@G-QCSFP had an irregular and porous network structure, and the DFO@G were dispersed in the hydrogel. FTIR spectroscopy was also utilized to confirm the chemical structure of CS, QCS, QCSF, and QCSFP hydrogel. As shown in Fig. 2d, the fresh peak at 1480 cm^{-1} of QCS was contributed to the methyl group of GTMAC, indicating the success of quaternization modification [51]. Compared with QCS, new peaks at 1352 and 804 cm^{-1} were contributed to B–O stretching vibration and benzene ring, respectively [52]. These peaks revealed that QCSF was successfully synthesized. Besides, the formation of boronic ester bonds could be proved by the two new peaks at 1431 cm^{-1} and 1734 cm^{-1}, which indicated that the boronic ester bonds cross-linked hydrogel was successfully prepared [53].

3.2. Responsive degradation behavior of hydrogel

In addition to the high glucose of the wound sites, enormous ROS were generated on the wound sites under physical and chemical effects [54]. Because the boronic ester bonds-based hydrogel could respond to the H_2O_2 and glucose of the wound microenvironment [55–57], the responsive degradation behaviors of the hydrogel were investigated. The results in Fig. 2e showed that after being incubated in a glucose environment for 24 h, the remaining weight of dry hydrogel was 35.3%, which revealed a higher degradation rate than the blank group. The hydrogel degradation was accelerated in the H_2O_2 environment and the remaining hydrogel was only 3.9% after incubation for 16 h, demonstrating the ROS-responsive ability of QCSFP hydrogel. When the hydrogel was incubated in the H_2O_2 and glucose environment, it showed the fastest degradation rate and the hydrogel could be almost cleared within 8 h. Since the boronic ester bonds are sensitive to the change of pH, the pH-dependent degradation behavior of the hydrogel was also evaluated at pH 6.0 and 7.8 to stimulate the healed and non-healing wound [43], respectively (Figure S7a). It was found that lower pH accelerated the degradation of the hydrogel. These results demonstrated that the hydrogel could respond to the ROS, glucose, and pH of the wound microenvironment, suggesting the QCSFP hydrogel had excellent wound microenvironment-responsive ability.

3.3. MMP-9 responsive drug release analysis

MMP-9, as a primary gelatinase, plays a critical role in ECM reorganization during the wound healing process. In diabetic wounds, MMP-9 is always overexpressed in the microenvironment [7,8,58]. To investigate the MMP-9 responsive release of DFO from the DFO@G microspheres, an *in vitro* experiment was conducted. As shown in Fig. 2f, without the DFO@G system, DFO-QCSFP hydrogel revealed a rapid drug release behavior (91% drug release) after 96 h. When adding the DFO@G system based on gelatin microspheres, the released drug of DFO@G-QCSFP reduced to 31% after 96 h, which indicated that the DFO@G could efficiently slow down the rate of drug release. Furthermore, the releasing rate of DFO@G-QCSFP was much more accelerated (56% drug release after 96 h) when incubated with overexpression of MMP-9 (100 ng mL^{-1} to simulate the diabetic wounds), suggesting that the DFO@G-QCSFP could respond to the high expression of MMP-9 in wound sites and achieve controlled drug release. Therefore, the results demonstrated that through the response of DFO@G to the overexpressed MMP-9, the DFO@G-QCSFP hydrogel could achieve controlled drug release, which guaranteed the effective time of drug on the wound sites while reducing the drug toxicity under safety control.

3.4. ROS scavenging ability evaluation

Extensive production of ROS in diabetic wounds impedes wound healing. The H_2O_2 scavenging ability of the hydrogel was evaluated and showed in Fig. 2g and S7b. After incubated with the hydrogel, the absorption intensity of the H_2O_2 solution was significantly reduced as the incubation time increased. We found that 200 μL of the hydrogel could eliminate 55% of H_2O_2 within 16 h (Fig. 2h). In addition, with increasing the amount of the hydrogel, the removed H_2O_2 was also increased to 69% within 16 h. To further investigate the ROS-scavenging ability of the hydrogel on the diabetic wound sites, 1 mM H_2O_2 and 16.6 mM glucose were used to be incubated with the hydrogel. The results showed that nearly 68% of H_2O_2 was eliminated after incubated for 16 h, indicating that the hydrogel could efficiently reduce the amount of the H_2O_2 in a high glucose environment. Meanwhile, the ROS-scavenging ability of the hydrogel against the hydroxyl radical (·OH) was also evaluated by using MB as the ·OH) indicator. The color of MB solution turned from blue to dark green when ·OH was produced by Fenton reaction, demonstrating the ·OH generation (Figure S7c). The absorption intensity of the ·OH solution was significantly reduced compared with the MB solution (Fig. 2i). After incubated with the hydrogel, the absorption intensity increased, suggesting that the hydrogel had an outstanding ·OH-scavenging ability. Additionally, DFO was known to improve the interaction between HIF-1α and coactivator p300 by scavenging hydroxyl radical-generating free iron Fe^{2+} [38], thus the ·OH-scavenging experiment of DFO was conducted (Figure S7d). As shown, with the increase of DFO concentration, the ·OH-scavenging ability was enhanced. All the above results demonstrated that effective ROS-scavenging activity could probably enable the hydrogel to reduce the ROS level in the wound sites. The responsive degradation, controlled drug release, and ROS-scavenging capacity of the hydrogel suggested a remarkable self-adaption behavior when applied in the diabetic wound microenvironment.

3.5. Rheological behavior, self-healing and injectable properties of hydrogel

Dynamic bonds crosslinked hydrogels usually showed promising properties that matched the elastic modulus of biological tissues [59]. In rheological analysis, gel point, which represented the critical state between solid and liquid, was defined as the cross point of storage modulus (G′) and loss modulus (G″). Dynamic frequency-sweep tests were carried out to prove the hydrogel formation of QCSFP and DFO@G-QCSFFP (Fig. 3a and **d**). From low frequency to high frequency, G′ was greater than G" for all samples, indicating a gel-like character. Furthermore, strain-dependent oscillatory measurements were applied to determine the critical strains for disrupting the gel network of QCSFP and DFO@G-QCSFP, found here to be 270.6% and 435.1%, respectively (Figure S8a and S8b). Hydrogel with self-healing ability could greatly maintain stability when subjected to external mechanical forces. The self-healing properties of QCSFP and DFO@G-QCSFP were quantitatively examined by using step-strain measurements (Fig. 3b and **e**). Based on the critical points, 500% was chosen as large strain while small strains were fixed at 1%. For both samples, G′ was greater than G″ when under small strain. As the strain was switched to 500%, G″ was higher than G′, indicating the collapse of the hydrogel. When small strain processed again, G′ and G″ recovered, revealing the network of hydrogel restored. In addition, the moduli had no noticeable change during three cycles, demonstrating the repeatable mechanical self-healing property of QCSFP and DFO@G-QCSFP hydrogels. The effect of high shear rate on gel viscosity was measured to evaluate the injectability of the QCSFP and DFO@G-QCSFP (Fig. 3c and **f**). As expected, for both samples, the viscosity decreased with the increase of shear rate, demonstrating that the shear disrupted the dynamic cross-links in the gel network. Additionally, the injectable ability was visualized by injecting the hydrogel through a needle (Fig. 3c inset).

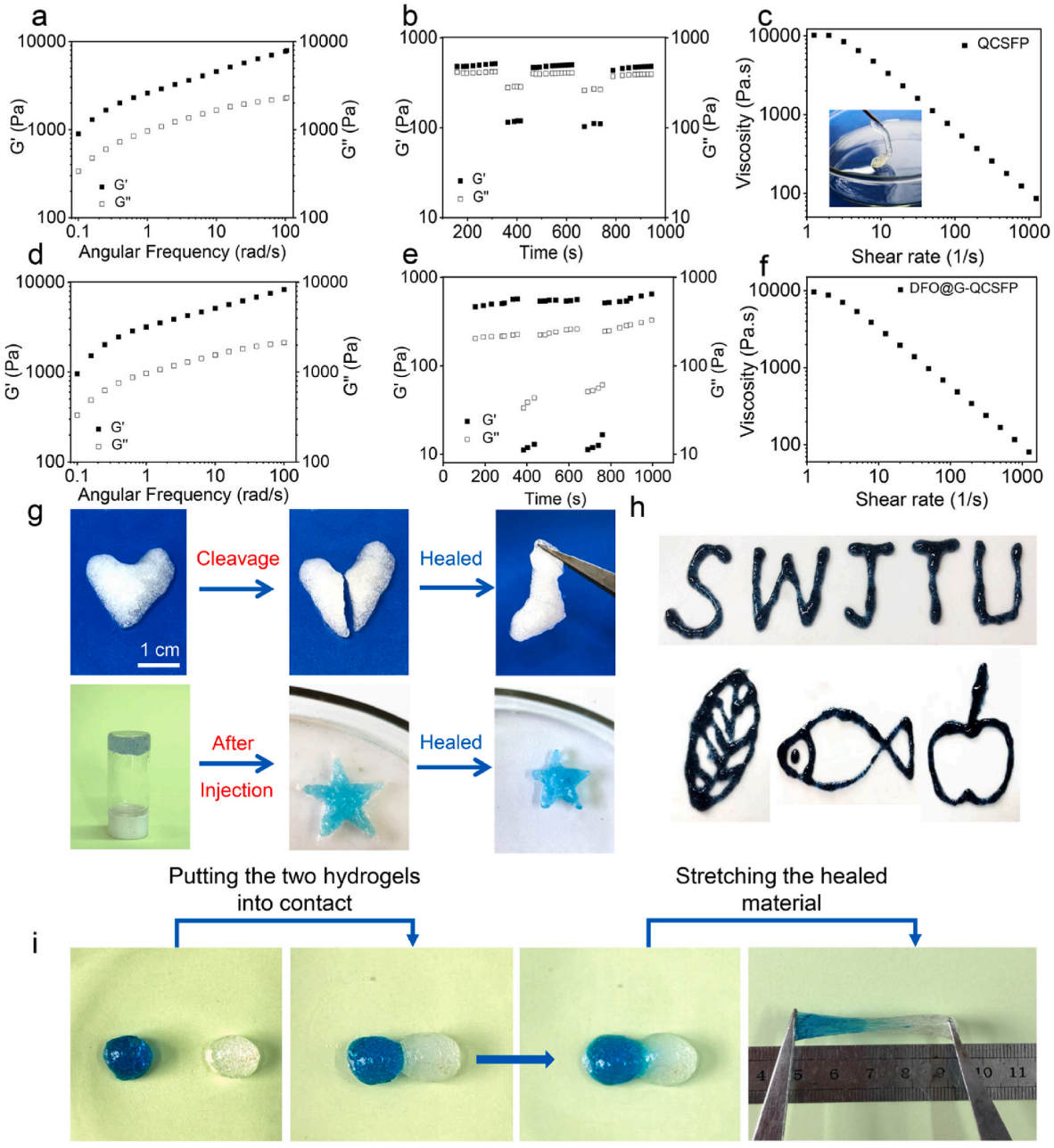

Fig. 3. Self-healing and injectable properties of the QCSFP and DFO@G-QCSFP hydrogels. a) Dynamic frequency-sweep measurements of the QCSFP hydrogel. b) Step-strain measurements to confirm self-healing capacity of the QCSFP hydrogel. c) Shear-thinning behavior of the QCSFP hydrogel. d) Dynamic frequency-sweep measurements of the d DFO@G-QCSFP hydrogel. e) Step-strain measurements to confirm self-healing capacity of the DFO@G-QCSFP hydrogel. f) Shear-thinning behavior of the DFO@G-QCSFP hydrogel. g) Optical images of the injection and healing processes. h) Reinjection of DFO@G-QCSFP into different shapes. i) Optical images of the self-healing process of two individual hydrogel blocks, in which the left block was stained with MB.

The self-healing and injectable capacities of the samples were also macroscopically evaluated. The QCSFP hydrogel was injected into a heart shape by a syringe and a crack was cut in the middle, then the two pieces of hydrogel were patched (Fig. 3g). The cracked hydrogel could recombine into a heart shape in 10 min without any stimuli. Furthermore, the QCSFP and DFO@G-QCSFP hydrogel could be repeatably injected into different shapes (Fig. 3g and **h**). Moreover, two independent hydrogel blocks were contacted and then stretched to visually investigate the self-healing properties (Fig. 3i). After being recombined for 2 h, the blocks became an integrated one and could maintain an integrated shape under stretching, indicating excellent self-healing ability of the hydrogels.

3.6. Cytocompatibility of the hydrogel

The cytotoxicity of the DFO@G and DFO@G-QCSFP hydrogel was assessed by AB assay and Live/Dead staining. After incubated with HUVECs for 1, 3 and 5 d at 37 °C, both two samples revealed no significant cytotoxicity and the cell viability was higher than 85% after 5 d incubation (Fig. 4a). In addition, the cell cytotoxicity was visually observed by the Live/Dead staining, in which the green and red fluorescence represented the live and dead cells, respectively (Fig. 4b). For all the samples, the majority of HUVECs showed normal morphology. It was observed that DFO@G and DFO@G-QCSFP groups revealed no difference in cell density from the control group. Hence, it could be concluded that the hydrogel possessed good cytocompatibility and could

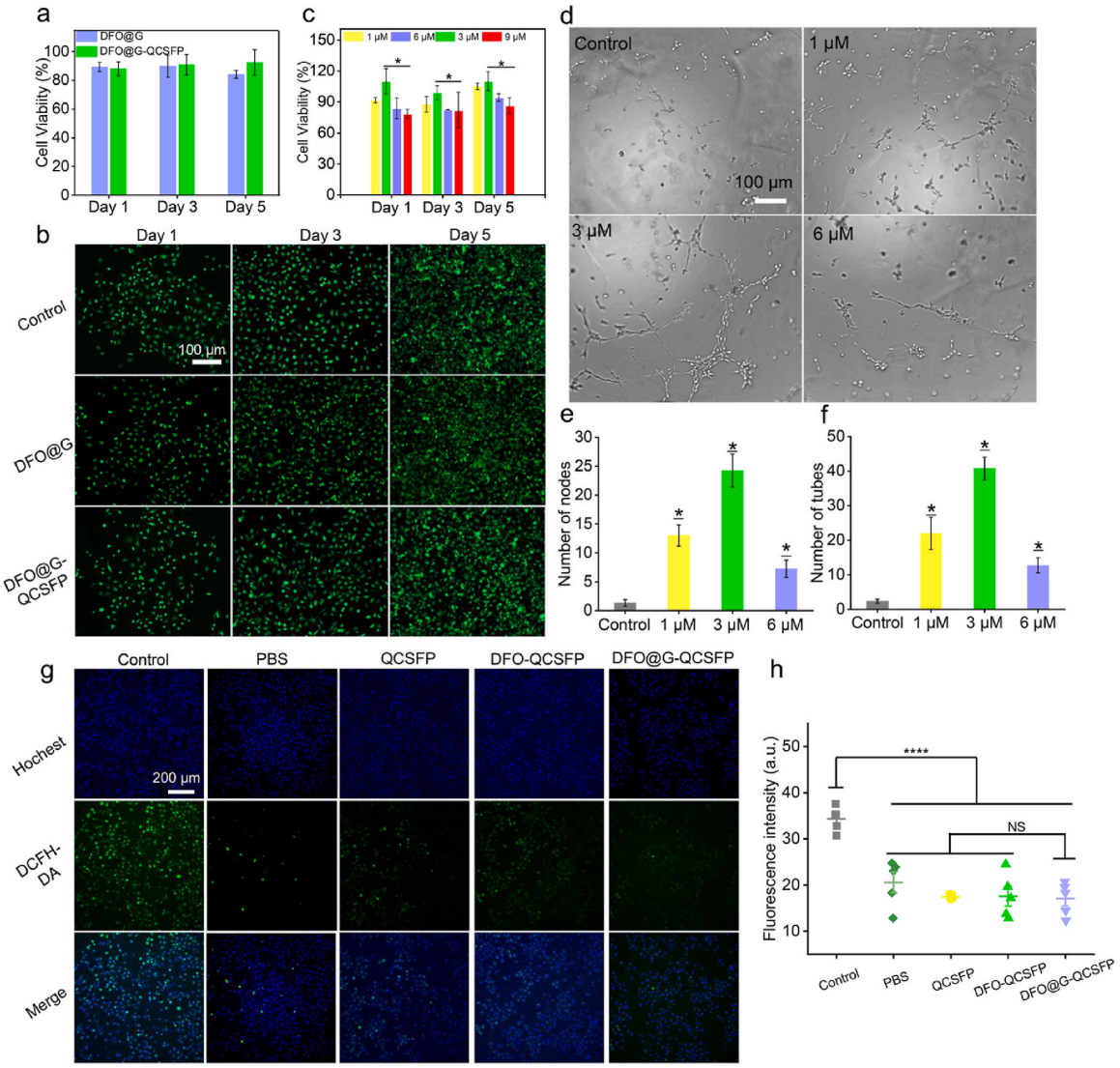

Fig. 4. Cell viability of HUVEC cells and tube formation to assess the *in vitro* angiogenesis capacity. a) Cell viability of HUVEC cells treated with DFO@G and DFO@G-QCSFP hydrogel for 1, 3, 5 d. b) Live/Dead staining of HUVEC cells after being treated with hydrogels for different time intervals. c) Cell viability after being treated with different concentrations of DFO. d) Optical images of tube formation by HUVEC cells treated with different concentrations of DFO, and quantification through counting the number of (e) nodes (n = 4) and (f) meshes (n = 4) in each group. g) The alleviation of oxidative stress in HUVECs was monitored via a DCFH-DA after different treatment. h) The quantitative studies of ROS decreasing intracellularly were analyzed by quantify the fluorescent intensity.

be used as a dressing for in vivo wound healing.

3.7. Effect of DFO concentration on tube formation and cytocompatibility

The concentration of DFO has an impact on cell proliferation. Thus, AB assay was performed on 1, 3, 6, and 9 μM DFO to investigate the relationship between DFO concentration and cytocompatibility (Fig. 4c). It could be noticed that with the increase of the DFO concentration, the cell viability first raised then decreased. Compared with the groups with lower concentrations, DFO with 6 μM and above concentration showed obvious cytotoxicity on HUVECs. In particular, DFO with 3 μM presented the effect of promoting cell proliferation with cell viability of 109% after incubated for 5 d while 9 μM of DFO revealed a cell viability of 86.1%. Moreover, DFO is proved to promote angiogenesis. To determine an effective concentration of DFO for promoting blood vessel formation, a tube formation assay was conducted. As shown in Fig. 4d, the angiogenesis capacity was significantly enhanced by adding DFO with concentrations of 1, 3, and 6 μM compared to the control group, as 9 μM showed a decreased cytotoxicity, it was not chosen for the tube formation assay. In addition, the concentration of 3 μM presented the higher stimulatory effects on tube formation, which showed 40 tubes and 20 nodes. The results demonstrated that DFO with a concentration of 3 μM possessed significant enhancement on both cell proliferation and tube formation.

3.8. Intracellular ROS-scavenging evaluation

To certificate the ability of DFO@G-QCSFP to decrease ROS level, the ROS-scavenging evaluation was conducted using the DCFH-DA probe. As shown in Fig. 4g and **h**, the intracellular ROS levels in hydrogel incubated groups were significantly decreased contrasted to the control group, in which cells presented prominent green fluorescence. The reason that three hydrogel groups presented similar ROS-scavenging abilities mainly due to the consistent content of phenylboronic acid groups in the hydrogel components, which were contributed to the ROS-scavenging. In summary, these results confirmed that the DFO@G-QCSFP hydrogel was sufficient to scavenge ROS thus alleviate the oxidative stress.

3.9. *In vivo* diabetic wound healing assessment

As a non-healing wound, a diabetic wound requires specific medical treatment owing to its complicated microenvironment [60]. The designed DFO@G-QCSFP hydrogel possessed the desired properties as a self-adaptive wound dressing for diabetic wounds. The treatment efficiency of DFO@G-QCSFP hydrogel was evaluated on a full-thickness diabetic wound model, which was established on SD rats through intraperitoneal injection of STZ. The details of the treatment were summarized in Fig. 5a. After the wounds with a diameter of 10 mm were formed, QCSFP, DFO-QCSFP, and DFO@G-QCSFP hydrogels were applied on the wound sites while the untreated wound was used as a control group. At specific time intervals, images of the wounds treated with different groups were shown in Fig. 5b. The treatment efficiency of DFO@G-QCSFP was much higher than other groups after 10 d observation. In addition, the wound healing traces were drawn based on the representative photos to show the treatment efficiency macroscopically. As shown in Fig. 5c and **d**, the wound area of each group was evaluated after 10 d of treatment. In the control group, the wound area remained as high as 38.1%, which was only remained 5.1% for the DFO@G-QCSFP group. Furthermore, the wound contraction during 20 d of treatment was monitored. As shown in Fig. 5e and Figure S9, it was observed that on the 14th day the wound contraction was 99.7% of the DFO@G-QCSFP group, which was superior to the QCSFP, DFO-QCSFP, and control group. These results indicated the DFO@G-QCSFP had faster healing rates than other groups. The mechanism of wound healing was then investigated by histological analysis in the next section.

3.10. *Histological analysis*

H&E and MT staining were conducted on the regenerated skin tissues to evaluate the healing effect from a histological perspective. As shown in Fig. 5f and **h**, the H&E stained sections revealed an inflammatory response and inflammatory cells were observed on the edge of the wound. After treatment with hydrogel dressings, the thickness of the epidermal layer of the wound sites was thicker than the control group (Fig. 5g). Among them, DFO@G-QCSFP showed the highest thickness at 101 μm, indicating a significant enhancement of epidermal layer formation of the hydrogel was conducive to wound healing. The deposition of collagen was detected on the regenerated skin tissues which were collected on day 10 by MT staining. It was observed that all the hydrogel groups exhibited higher collagen deposition than the control group (Fig. 5i). In addition, DFO@G-QCSFP presented the densest collagen deposition at 55%, which was 1.71-fold higher than that of the control group. Compared to the DFO-QCSFP group, it also revealed significant acceleration on epithelization and collagen deposition, which demonstrated that the DFO@G-QCSFP hydrogel could accelerate the diabetic wound healing through the promotion of collagen deposition.

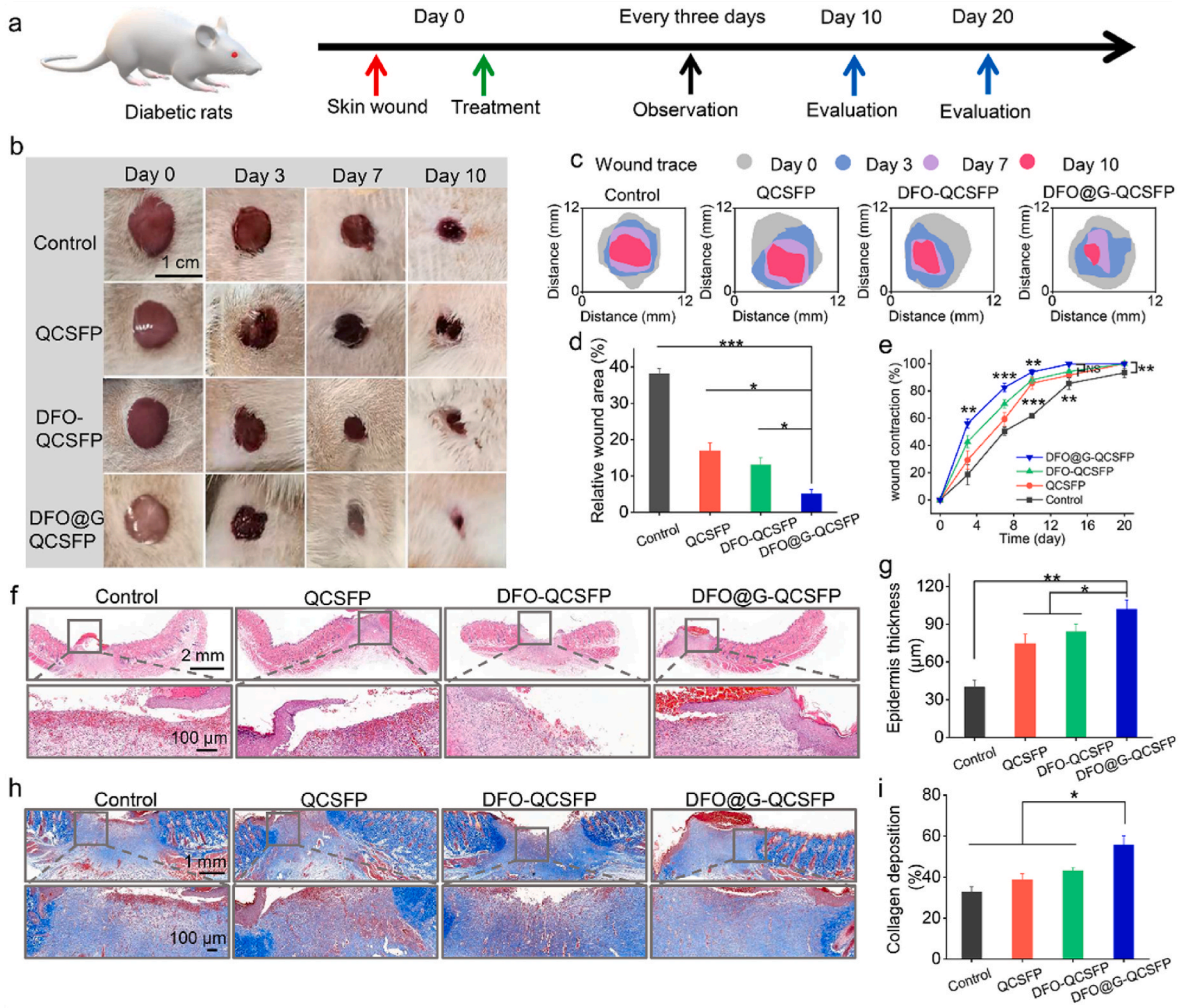

Fig. 5. *In vivo* diabetic wound healing assessment of multifunctional hydrogels. a) Treatment schedule of diabetic wounds treated by different hydrogel formulations. b) Representative images of the diabetic wounds at different times. c) Wound traces of the healing process. d) Quantification of relative wound area on day 10 after treatment. e) Quantification of wound contraction during the healing process. f) H&E staining of wound sections in all groups on day 10. g) Epidermis thickness on day 10. h) MT images of wounds on day 10. i) Collagen accumulation on day 10 based on MT staining. *p < 0.05, **p < 0.01, ***p < 0.001.

Besides collagen deposition, angiogenesis is also crucial for diabetic wound healing since the growth of the newly-formed granulation tissue was very dependent on the nutrition, which was provided by the blood vessels [61]. To visually examine the angiogenesis effect of hydrogels, IHC staining of HIF-1α and VEGF was performed. As shown in Fig. 6a and **c**, the staining of HIF-1α and VEGF was the deepest in the DFO@G-QCSFP group, demonstrating this group had the highest expressions of HIF-1α and VEGF than other groups. IHC evaluation statistical analysis of HIF-1α and VEGF was also performed to confirm the angiogenesis effect. The results in Fig. 6b and **d** revealed that the expression of HIF-1α and VEGF was increased after adding DFO in the wound sites. In addition, the controlled release system of DFO@G-QCSFP could significantly enhance the expressions, with the IHC scores of DFO@G-QCSFP 3.81-folder (HIF-1α) and 2.88-folder (VEGF) than the control group on day 10. The intensity of staining was similar across the hydrogel groups without significant difference on day 20. Because the healing process was almost completed while the control group showed increased expression on day 20. The reason was probably due to that the wound treated by DFO@G-QCSFP returned to a regular state in day 20 so the expression of α-SMA and CD31 was on a normal level. In the meantime, the control group was still in the healing process in day 20, which presented a high expression of α-SMA and CD31, which showed a similar tendency with previous literature [47].

CD31 is a transmembrane protein expressed in early angiogenesis, thus its expression could be evaluated to illustrate the newly formed blood vessels. IHC staining of α-SMA and CD31 was conducted as shown in Fig. 6e and **h**. It was observed that DFO@G-QCSFP had the highest expressions of α-SMA (Fig. 6f), consistent with the results of HIF-1α and VEGF staining. Furthermore, as shown in Fig. 6h, the newly formed blood vessels were counted from the CD31 staining and the results showed the DFO@G-QCSFP had the highest number of blood vessels at 71 vessels mm^{-2} on day 10, which was 2.65-folder than the control group. The results indicated that the DFO@G-QCSFP exhibited excellent pro-vascularization capability.

The in vivo ROS-scavenging ability of DFO@G-QCSFP was conducted as well. As shown in Figure S10, it could be observed that all the hydrogel treated groups presented a good ROS-scavenging ability compared to the control group in day 1. No significant difference

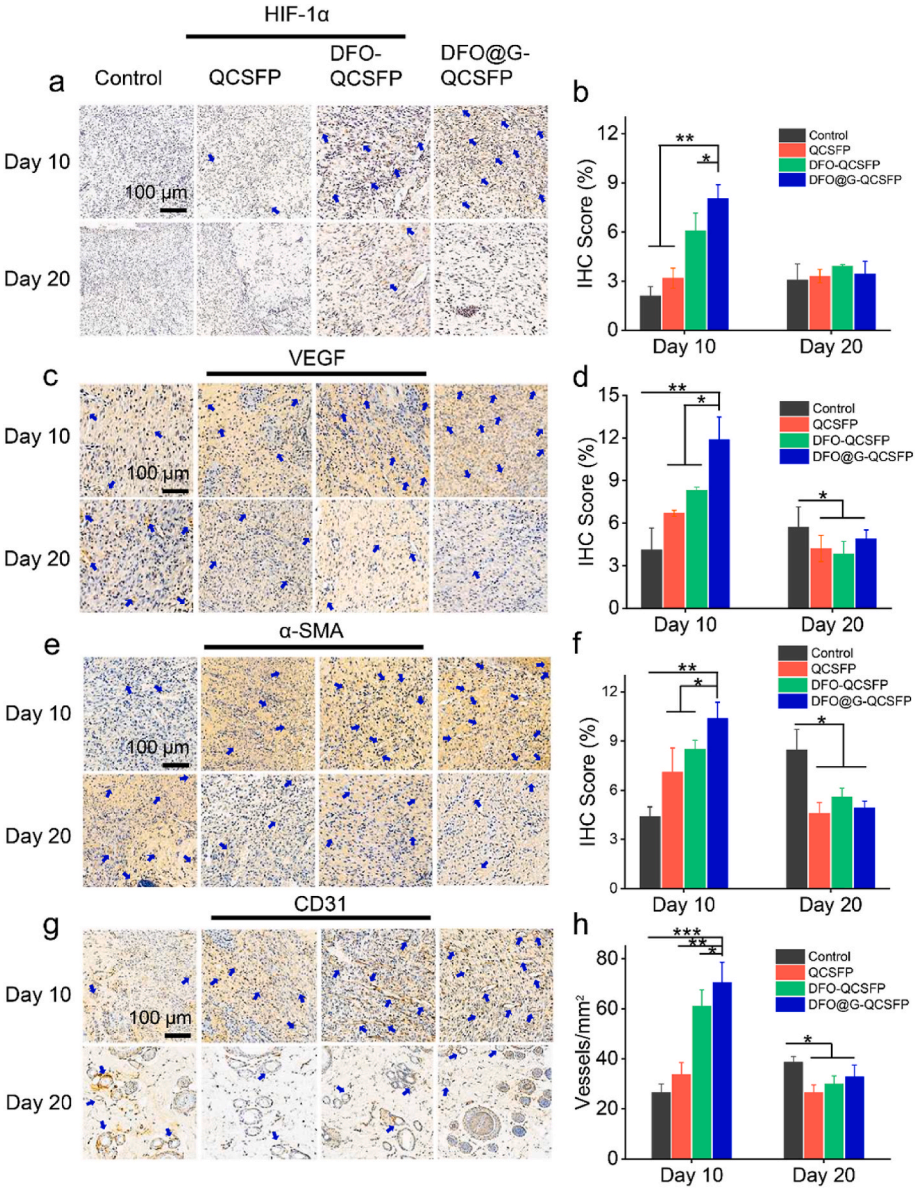

Fig. 6. IHC staining and quantification of a), b) HIF-1α, c), d) VEGF, e), f) α-SMA and g) CD31, h) Quantification of blood vessels from CD31 staining. *$p < 0.05$, **$p < 0.01$, ***$p < 0.001$.

between the three hydrogel groups was owing to the same amount of boronate ester bonds, which contributed the most to ROS-scavenging. Followed 3 days of treatment, DFO@G-QCSFP revealed a significant elimination of ROS than other groups mainly because of the sustained release of DFO helped to reduce the ROS level by chelation with Fe^{2+}. The results demonstrated that the DFO@G-QCSFP could efficiently accelerate wound healing by reducing ROS levels in diabetic wounds. The in vivo degradation of the hydrogel was conducted and the result was shown in Figure S11. After applying in the wound, the hydrogel revealed a fast degradation behavior. The remaining hydrogel after 24 h was 34.78% and decreased to 9.5% after 36 h.

Moreover, the self-adaptive hydrogel dressings were supposed to change the microenvironment to a pro-healing state by eliminating ROS and promoting angiogenesis. Therefore, IHC staining of MMP-9 and Ki67 was detected to investigate the microenvironment of the wounds treated by different groups. The results revealed that the control group had the highest expression of MMP-9, which was consistent with the pathological characteristics of diabetic wounds (Figure S12a). After being treated with QCSFP, DFO-QCSFP and DFO@G-QCSFP, the expressions were decreased. IHC evaluation statistical analysis results demonstrated that after treatment, DFO@G-QCSFP showed the most apparent effect on reducing the expression of MMP-9, which was 1.86-folder less than the control group at day 10 (Figure S12b). IHC staining and evaluation statistical analysis of Ki67 was also detected to confirm the change of the microenvironment after treatment (Figure S12c and S12d). It could be observed that DFO@G-QCSFP showed the highest expression of Ki67, indicating its ability to promote cell proliferation. These results demonstrated that after being treated with DFO@G-QCSFP hydrogel, the microenvironment of the wound could be changed to a pro-healing state by regulating the ROS level, promoting collagen deposition and cell proliferation, improving vascularization and decreasing the expression of MMP-9.

4. Conclusion

In summary, a microenvironment self-adaptive hydrogel based on boronic ester bonds was constructed to accelerate diabetic wound healing by dynamically regulating the microenvironment through ROS scavenging and on-demand DFO release to promote angiogenesis. Owing to the dynamic nature of the boronic ester bonds, the hydrogel revealed excellent self-healing capability, injectability as well as the wound microenvironment perception self-adaptive ability. As well, the hydrogel could eliminate 68% of H_2O_2, revealing good ROS-scavenging ability. Meanwhile, the DFO@G released from the hydrogel could respond to the overexpressed MMP-9, achieving an on-demand release of DFO. A full-thickness diabetic wound exhibited a reduced wound area of only 5.1% after 10 days' treatment with this hydrogel. Furthermore, the hydrogel reshaped the microenvironment to a pro-healing state to accelerate wound healing. As a wound microenvironment self-adaptive multifunctional wound dressing, this hydrogel possesses a potential for the treatment of diabetic wounds and skin tissue regeneration.

Ethics approval and consent to participate

The authors declare that all animal experiments are carried out according to the guidelines approved by the Institutional Animal Care and Use Committee of Southwest Jiaotong University (No. SWJTU-2013-008). All authors comply with all relevant ethical regulations.

CRediT authorship contribution statement

Zijian Shao: Conceptualization, Methodology, Software, Data curation, Investigation, Writing – original draft. **Tianyu Yin:** Data curation, Investigation, Writing – original draft. **Jinbo Jiang:** Visualization, Investigation. **Yang He:** Visualization, Investigation. **Tao Xiang:** Data curation, Investigation, Writing – original draft, Funding acquisition, Writing – review & editing. **Shaobing Zhou:** Funding acquisition, Writing – review & editing.

Declaration of competing interest

The authors declare that they have no known competing financial interests or personal relationships that could have appeared to influence the work reported in this paper.

Acknowledgements

This work was supported by the National Natural Science Foundation of China (Nos. 52103186, 51725303 and 52033007), the Fundamental Research Funds for the Central Universities (Nos. 2682020ZT84 and 2682021ZTPY008). The authors also thank the Analytical and Testing Center of Southwest Jiaotong University.

Appendix A. Supplementary data

Supplementary data to this article can be found online at https://doi.org/10.1016/j.bioactmat.2022.06.018.

References

[1] H. Wang, Z. Xu, M. Zhao, G. Liu, J. Wu, Advances of hydrogel dressings in diabetic wounds, Biomater. Sci. 9 (5) (2021) 1530–1546, https://doi.org/10.1039/D0BM01747G.
[2] G.C. Gurtner, S. Werner, Y. Barrandon, M.T. Longaker, Wound repair and regeneration, Nature 453 (7193) (2008) 314–321, https://doi.org/10.1038/nature07039.
[3] V. Falanga, Wound healing and its impairment in the diabetic foot, Lancet 366 (9498) (2005) 1736–1743, https://doi.org/10.1016/S0140-6736(05)67700-8.
[4] C. Tong, X. Zhong, Y. Yang, X. Liu, G. Zhong, C. Xiao, B. Liu, W. Wang, X. Yang, Pb@pda@ag nanosystem for synergistically eradicating mrsa and accelerating diabetic wound healing assisted with laser irradiation, Biomaterials 243 (2020), 119936, https://doi.org/10.1016/j.biomaterials.2020.119936.
[5] W.-C. Huang, R. Ying, W. Wang, Y. Guo, Y. He, X. Mo, C. Xue, X. Mao, A macroporous hydrogel dressing with enhanced antibacterial and anti-inflammatory capabilities for accelerated wound healing, Adv. Funct. Mater. 30 (21) (2020), 2000644, https://doi.org/10.1002/adfm.202000644.
[6] L. Wang, X. Zhang, K. Yang, Y.V. Fu, T. Xu, S. Li, D. Zhang, L.-N. Wang, C.-S. Lee, A novel double-crosslinking-double-network design for injectable hydrogels with enhanced tissue adhesion and antibacterial capability for wound treatment, Adv. Funct. Mater. 30 (1) (2020), 1904156, https://doi.org/10.1002/adfm.201904156.
[7] J. Liu, Z. Chen, J. Wang, R. Li, T. Li, M. Chang, F. Yan, Y. Wang, Encapsulation of curcumin nanoparticles with mmp9-responsive and thermos-sensitive hydrogel improves diabetic wound healing, ACS Appl. Mater. Interfaces 10 (19) (2018) 16315–16326, https://doi.org/10.1021/acsami.8b03868.
[8] S.A. Castleberry, B.D. Almquist, W. Li, T. Reis, J. Chow, S. Mayner, P.T. Hammond, Self-assembled wound dressings silence mmp-9 and improve diabetic wound healing in vivo, Adv. Mater. 28 (9) (2016) 1809–1817, https://doi.org/10.1002/adma.201503565.
[9] Z. Tu, M. Chen, M. Wang, Z. Shao, X. Jiang, K. Wang, Z. Yao, S. Yang, X. Zhang, W. Gao, C. Lin, B. Lei, C. Mao, Engineering bioactive M2 macrophage-polarized anti-inflammatory, antioxidant, and antibacterial scaffolds for rapid angiogenesis and diabetic wound repair, Adv. Funct. Mater. 31 (2021), 2100924, https://doi.org/10.1002/adfm.202100924.
[10] X. Zheng, S. Narayanan, V.G. Sunkari, S. Eliasson, I.R. Botusan, J. Grunler, A. I. Catrina, F. Radtke, C. Xu, A. Zhao, N.R. Ekberg, U. Lendahl, S.-B. Catrina, Triggering of a dll4-notch1 loop impairs wound healing in diabetes, Proc. Natl. Acad. Sci. USA 116 (14) (2019) 6985–6994, https://doi.org/10.1073/pnas.1900351116.
[11] M. Wang, M. Chen, W. Niu, D.D. Winston, W. Cheng, B. Lei, Injectable biodegradation-visual self-healing citrate hydrogel with high tissue penetration for microenvironment-responsive degradation and local tumor therapy, Biomaterials 261 (2020), 120301, https://doi.org/10.1016/j.biomaterials.2020.120301.
[12] F. Qian, Y. Han, Z. Han, D. Zhang, L. Zhang, G. Zhao, S. Li, G. Jin, R. Yu, H. Liu, In situ implantable, post-trauma microenvironment-responsive, ros depletion hydrogels for the treatment of traumatic brain injury, Biomaterials 270 (2021), 120675, https://doi.org/10.1016/j.biomaterials.2021.120675.
[13] S. Xue, X. Li, S. Li, N. Chen, Q. Zhan, L. Long, J. Zhao, X. Hou, X. Yuan, Bone fracture microenvironment responsive hydrogel for timing sequential release of cargoes, Colloids Surf., A 629 (2021), 127413, https://doi.org/10.1016/j.colsurfa.2021.127413.
[14] B. Yu, C. He, W. Wang, Y. Ren, J. Yang, S. Guo, Y. Zheng, X. Shi, Asymmetric wettable composite wound dressing prepared by electrospinning with bioinspired micropatterning enhances diabetic wound healing, ACS Appl. Bio Mater. 3 (8) (2020) 5383–5394, https://doi.org/10.1021/acsabm.0c00695.

[15] M. Li, J. Chen, M. Shi, H. Zhang, P.X. Ma, B. Guo, Electroactive anti-oxidant polyurethane elastomers with shape memory property as non-adherent wound dressing to enhance wound healing, Chem. Eng. J. 375 (2019), 121999, https://doi.org/10.1016/j.cej.2019.121999.
[16] F.V. Ferreira, C.G. Otoni, K.J. De France, H.S. Barud, L.M.F. Lona, E.D. Cranston, O. J. Rojas, Porous nanocellulose gels and foams: breakthrough status in the development of scaffolds for tissue engineering, Mater, Today Off. 37 (2020) 126–141, https://doi.org/10.1016/j.mattod.2020.03.003.
[17] X. Ding, G. Li, P. Zhang, E. Jin, C. Xiao, X. Chen, Injectable self-healing hydrogel wound dressing with cysteine-specific on-demand dissolution property based on tandem dynamic covalent bonds, Adv. Funct. Mater. 31 (19) (2021), https://doi.org/10.1002/adfm.202011230, 2011230.
[18] X. Zhao, Y. Liang, Y. Huang, J. He, Y. Han, B. Guo, Physical double-network hydrogel adhesives with rapid shape adaptability, fast self-healing, antioxidant and NIR/pH stimulus-responsiveness for multidrug-resistant bacterial infection and removable wound dressing, Adv. Funct. Mater. 30 (17) (2020), 1910748, https://doi.org/10.1002/adfm.201910748.
[19] M.A.M. Jahromi, P.S. Zangabad, S.M.M. Basri, K.S. Zangabad, A. Ghamarypour, A. R. Aref, M. Karimi, M.R. Hamblin, Nanomedicine and advanced technologies for burns: preventing infection and facilitating wound healing, Adv. Drug Deliv. Rev. 123 (2018) 33–64, https://doi.org/10.1016/j.addr.2017.08.001.
[20] X. Chen, Making electrodes stretchable, Small Methods 1 (4) (2017), 1600029, https://doi.org/10.1002/smtd.201600029.
[21] J. Li, F. Yu, G. Chen, J. Liu, X.-L. Li, B. Cheng, X.-M. Mo, C. Chen, J.-F. Pan, Moist-retaining, self-recoverable, bioadhesive, and transparent in situ forming hydrogels to accelerate wound healing, ACS Appl. Mater. Interfaces 12 (2) (2020) 2023–2038, https://doi.org/10.1021/acsami.9b17180.
[22] H. Chen, R. Cheng, X. Zhao, Y. Zhang, A. Tam, Y. Yan, H. Shen, Y.S. Zhang, J. Qi, Y. Feng, L. Liu, G. Pan, W. Cui, L. Deng, An injectable self-healing coordinative hydrogel with antibacterial and angiogenic properties for diabetic skin wound repair, NPG Asia Mater. 11 (2019) 3, https://doi.org/10.1038/s41427-018-0103-9.
[23] T. Chen, Y. Chen, H.U. Rehman, Z. Chen, Z. Yang, M. Wang, H. Li, H. Liu, Ultratough, self-healing, and tissue-adhesive hydrogel for wound dressing, ACS Appl. Mater. Interfaces 10 (39) (2018) 33523–33531, https://doi.org/10.1021/acsami.8b10064.
[24] H. Zhao, J. Huang, Y. Li, X. Lv, H. Zhou, H. Wang, Y. Xu, C. Wang, J. Wang, Z. Liu, ROS-scavenging hydrogel to promote healing of bacteria infected diabetic wounds, Biomaterials 258 (2020), 120286, https://doi.org/10.1016/j.biomaterials.2020.120286.
[25] S.-W. Kim, G.-B. Im, G.-J. Jeong, S. Baik, J. Hyun, Y.-J. Kim, C. Pang, Y.C. Jang, S. H. Bhang, Delivery of a spheroids-incorporated human dermal fibroblast sheet increases angiogenesis and M2 polarization for wound healing, Biomaterials 275 (2021) 120954, https://doi.org/10.1016/j.biomaterials.2021.120954.
[26] L. Li, B. Yan, J. Yang, L. Chen, H. Zeng, Novel mussel-inspired injectable self-healing hydrogel with anti-biofouling property, Adv. Mater. 27 (7) (2015) 1294–1299, https://doi.org/10.1002/adma.201405166.
[27] Q. Feng, K. Zhang, R. Li, L. Bian, Injectable hydrogels for regenerative medicine, Acta Polym. Sin. 52 (1) (2021) 1–15, https://doi.org/10.1007/s13770-018-0161-7.
[28] Y. Tu, N. Chen, C. Li, H. Liu, R. Zhu, S. Chen, Q. Xiao, J. Liu, S. Ramakrishna, L. He, Advances in injectable self-healing biomedical hydrogels, Acta Biomater. 90 (2019) 1–20, https://doi.org/10.1016/j.actbio.2019.03.057.
[29] R. Dimatteo, N.J. Darling, T. Segura, In situ forming injectable hydrogels for drug delivery and wound repair, Adv. Drug Deliv. Rev. 127 (2018) 167–184, https://doi.org/10.1016/j.addr.2018.03.007.
[30] R. Du, Z. Xu, C. Zhu, Y. Jiang, H. Yan, H.-C. Wu, O. Vardoulis, Y. Cai, X. Zhu, Z. Bao, Q. Zhang, X. Jia, A highly stretchable and self-healing supramolecular elastomer based on sliding crosslinks and hydrogen bonds, Adv. Funct. Mater. 30 (7) (2020), 1907139, https://doi.org/10.1002/adfm.201907139.
[31] S. Li, L. Wang, W. Zheng, G. Yang, X. Jiang, Rapid fabrication of self-healing, conductive, and injectable gel as dressings for healing wounds in stretchable parts of the body, Adv. Funct. Mater. 30 (31) (2020), 2002370, https://doi.org/10.1002/adfm.202002370.
[32] C. Hou, W. He, Z. Wang, B. Yi, Z. Hu, W. Wang, X. Deng, X. Yao, Particulate-aggregated adhesives with exudate-sensitive properties and sustained bacteria disinfection to facilitate wound healing, ACS Appl. Mater. Interfaces 12 (28) (2020) 31090–31098, https://doi.org/10.1021/acsami.0c04920.
[33] H. Mndlovu, L.C. du Toit, P. Kumar, T. Marimuthu, P.P.D. Kondiah, Y.E. Choonara, V. Pillay, Development of a fluid-absorptive alginate-chitosan bioplatform for potential application as a wound dressing, Carbohydr. Polym. 222 (2019), 114988, https://doi.org/10.1016/j.carbpol.2019.114988.
[34] S. Li, N. Chen, X. Li, Y. Li, Z. Xie, Z. Ma, J. Zhao, X. Hou, X. Yuan, Bioinspired double-dynamic-bond crosslinked bioadhesive enables post-wound closure care, Adv. Funct. Mater. 30 (17) (2020), 2000130, https://doi.org/10.1002/adfm.202000130.
[35] M. Wang, C. Wang, M. Chen, Y. Xi, W. Cheng, C. Mao, T. Xu, X. Zhang, C. Lin, W. Gao, Y. Guo, B. Lei, Efficient angiogenesis-based diabetic wound healing/skin reconstruction through bioactive antibacterial adhesive ultraviolet shielding nanodressing with exosome release, ACS Nano 13 (9) (2019) 10279–10293, https://doi.org/10.1021/acsnano.9b03656.
[36] X. Zhao, D. Pei, Y. Yang, K. Xu, J. Yu, Y. Zhang, Q. Zhang, G. He, Y. Zhang, A. Li, Y. Cheng, X. Chen, Green tea derivative driven smart hydrogels with desired functions for chronic diabetic wound treatment, Adv. Funct. Mater. 31 (2021), 2009442, https://doi.org/10.1002/adfm.202009442.
[37] V. Yesilyurt, M.J. Webber, E.A. Appel, C. Godwin, R. Langer, D.G. Anderson, Injectable self-healing glucose-responsive hydrogels with ph-regulated mechanical properties, Adv. Mater. 28 (1) (2016) 86–91, https://doi.org/10.1002/adma.201502902.
[38] H. Chen, P. Jia, H. Kang, H. Zhang, Y. Liu, P. Yang, Y. Yan, G. Zuo, L. Guo, M. Jiang, Upregulating HIF-1α by hydrogel nanofibrous scaffolds for rapidly recruiting angiogenesis relative cells in diabetic wound, Adv. Healthc. Mater. 5 (8) (2016) 907–918, https://doi.org/10.1002/adhm.201501018.
[39] H. Chen, L. Guo, J. Wicks, C. Ling, X. Zhao, Y. Yan, J. Qi, W. Cui, L. Deng, Quickly promoting angiogenesis by using a dfo-loaded photo-crosslinked gelatin hydrogel for diabetic skin regeneration, J. Mater. Chem. B 4 (21) (2016) 3770–3781, https://doi.org/10.1039/C6TB00065G.
[40] X. Zhao, P. Li, B.L. Guo, P.X. Ma, Antibacterial and conductive injectable hydrogels based on quaternized chitosan-graft-polyaniline/oxidized dextran for tissue engineering, Acta Biomater. 26 (2015) 236–248, https://doi.org/10.1016/j.actbio.2015.08.006.
[41] F. Xu, X. Li, X. Huang, J. Pan, Y. Wang, S. Zhou, Development of a ph-responsive polymersome inducing endoplasmic reticulum stress and autophagy blockade, Sci. Adv. 6 (31) (2020), https://doi.org/10.1126/sciadv.abb8725 eabb8725.
[42] L. Yuan, X. Li, L. Ge, X. Jia, J. Lei, C. Mu, D. Li, Emulsion template method for the fabrication of gelatin-based scaffold with a controllable pore structure, ACS Appl. Mater. Interfaces 11 (1) (2019) 269–277, https://doi.org/10.1021/acsami.8b17555.
[43] S.L. Percival, S. McCarty, J.A. Hunt, E.J. Woods, The effects of ph on wound healing, biofilms, and antimicrobial efficacy, Wound Repair Regen. 22 (2) (2014) 174–186, https://doi.org/10.1111/wrr.12125.
[44] R. Lobmann, A. Ambrosch, G. Schultz, K. Waldmann, S. Schiweck, H. Lehnert, Expression of matrix-metalloproteinases and their inhibitors in the wounds of diabetic and non-diabetic patients, Diabetologia 45 (7) (2002) 1011–1016, https://doi.org/10.1007/s00125-002-0868-8.
[45] Z. Li, S. Guo, F. Yao, Y. Zhang, T. Li, Increased ratio of serum matrix metalloproteinase-9 against TIMP-1 predicts poor wound healing in diabetic foot ulcers, J. Diabet. Complicat. 27 (4) (2013) 380–382, https://doi.org/10.1016/j.jdiacomp.2012.12.007.
[46] S. Wang, H. Zheng, L. Zhou, F. Cheng, Z. Liu, H. Zhang, L. Wang, Q. Zhang, Nanoenzyme-reinforced injectable hydrogel for healing diabetic wounds infected with multidrug resistant bacteria, Nano Lett. 20 (7) (2020) 5149–5158, https://doi.org/10.1021/acs.nanolett.0c01371.
[47] L. Kong, Z. Wu, H. Zhao, H. Cui, J. Shen, J. Chang, H. Li, Y. He, Bioactive injectable hydrogels containing desferrioxamine and bioglass for diabetic wound healing, ACS Appl. Mater. Interfaces 10 (36) (2018) 30103–30114, https://doi.org/10.1021/acsami.8b09191.
[48] M. Kharaziha, A. Baidya, N. Annabi, Rational design of immunomodulatory hydrogels for chronic wound healing, Adv. Mater. 33 (2021), 2100176, https://doi.org/10.1002/adma.202100176.
[49] J. Qu, X. Zhao, Y. Liang, T. Zhang, P.X. Ma, B. Guo, Antibacterial adhesive injectable hydrogels with rapid self-healing, extensibility and compressibility as wound dressing for joints skin wound healing, Biomaterials 183 (2018) 185–199, https://doi.org/10.1016/j.biomaterials.2018.08.044.
[50] L. Liu, M. Zhu, X. Xu, X. Li, Z. Ma, Z. Jiang, A. Pich, H. Wang, P. Song, Dynamic nanoconfinement enabled highly stretchable and supratough polymeric materials with desirable healability and biocompatibility, Adv. Mater. 33 (51) (2021), 2105829, https://doi.org/10.1002/adma.202105829.
[51] X. Zhao, B. Guo, H. Wu, Y. Liang, P.X. Ma, Injectable antibacterial conductive nanocomposite cryogels with rapid shape recovery for noncompressible hemorrhage and wound healing, Nat. Commun. 9 (2018) 2784, https://doi.org/10.1038/s41467-018-04998-9.
[52] S.H. Hong, S. Kim, J.P. Park, M. Shin, K. Kim, J.H. Ryu, H. Lee, Dynamic bonds between boronic acid and alginate: hydrogels with stretchable, self-healing, stimuli-responsive, remoldable, and adhesive properties, Biomacromolecules 19 (6) (2018) 2053–2061, https://doi.org/10.1021/acs.biomac.8b00144.
[53] C.C. Deng, W.L.A. Brooks, K.A. Abboud, B.S. Sumerlin, Boronic acid-based hydrogels undergo self-healing at neutral and acidic ph, ACS Macro Lett. 4 (2) (2015) 220–224, https://doi.org/10.1021/acsmacrolett.5b00018.
[54] T. Wang, Y. Li, E.J. Cornel, C. Li, J. Du, Combined antioxidant-antibiotic treatment for effectively healing infected diabetic wounds based on polymer vesicles, ACS Nano 15 (5) (2021) 9027–9038, https://doi.org/10.1021/acsnano.1c02102.
[55] B. Marco-Dufort, M.W. Tibbitt, Design of moldable hydrogels for biomedical applications using dynamic covalent boronic esters, Mater. Today Chem. 12 (2019) 16–33, https://doi.org/10.1016/j.mtchem.2018.12.001.
[56] B. Wang, K. Yoshida, K. Sato, J.-i. Anzai, Phenylboronic acid-functionalized layer-by-layer assemblies for biomedical applications, Polymers 9 (6) (2017) 202, https://doi.org/10.3390/polym9060202.
[57] Y.E. Kim, J. Kim, ROS-scavenging therapeutic hydrogels for modulation of the inflammatory response, ACS Appl. Mater. Interfaces 14 (20) (2022) 23002–23021, https://doi.org/10.1021/acsami.1c18261.
[58] J. Sonamuthu, Y. Cai, H. Liu, M.S.M. Kasim, V.R. Vasanthakumar, B. Pandi, H. Wang, J. Yao, MMP-9 responsive dipeptide-tempted natural protein hydrogel-based wound dressings for accelerated healing action of infected diabetic wound, Int. J. Biol. Macromol. 153 (2020) 1058–1069, https://doi.org/10.1016/j.ijbiomac.2019.10.236.
[59] S. Talebian, M. Mehrali, N. Taebnia, C.P. Pennisi, F.B. Kadumudi, J. Foroughi, M. Hasany, M. Nikkhah, M. Akbari, G. Orive, A. Dolatshahi-Pirouz, Self-healing

hydrogels: the next paradigm shift in tissue engineering? Adv. Sci. 6 (16) (2019), 1801664 https://doi.org/10.1002/advs.201801664.

[60] G. Han, R. Ceilley, Chronic wound healing: a review of current management and treatments, Adv. Ther. 34 (3) (2017) 599–610, https://doi.org/10.1007/s12325-017-0478-y.

[61] X. Zhang, G. Chen, Y. Liu, L. Sun, L. Sun, Y. Zhao, Black phosphorus-loaded separable microneedles as responsive oxygen delivery carriers for wound healing, ACS Nano 14 (5) (2020) 5901–5908, https://doi.org/10.1021/acsnano.0c01059.